Melting in two-dimensional systems: Characterizing continuous and first-order transitions

Óscar Toledano ⓘ,[1,*] M. Pancorbo ⓘ,[1] J. E. Alvarellos ⓘ,[2] and Óscar Gálvez ⓘ[1]

[1]*Departamento Física Interdisciplinar, Facultad de Ciencias, Universidad Nacional de Educación a Distancia (UNED), Senda del Rey, 9, 28040 Madrid, Spain*

[2]*Departamento Física Fundamental, Facultad de Ciencias, Universidad Nacional de Educación a Distancia (UNED), Senda del Rey, 9, 28040 Madrid, Spain*

The mechanisms underlying the melting process in bidimensional systems have been widely studied by means of experiments, theory, and simulations since Kosterlitz, Thouless, Halperin, Nelson, and Young elaborated the KTHNY theory. In the framework of this theory, melting is produced by two continuous transitions mediated by the unbinding of local defects and the appearance of an intermediate phase between solid and liquid, called "hexatic." There are also other competing theories that could explain this process, as, e.g., the formation of grain boundaries (lines of defects), which lead to a first-order transition. In this paper, simulations of systems interacting via the Lennard Jones 6–12 and Morse potentials using the Metropolis Monte Carlo method in the NVT ensemble have been performed to study the effect of the potential shape in the melting process. Additionally, truncated Morse potentials (with only a repulsive part) have been used to investigate the effect of the long-range interactions. Transitions from solid to hexatic phases were found to be continuous for all potentials studied, but transitions from hexatic to liquid phases were found to be either continuous or first order, depending on the thermodynamic conditions and the potential interaction selected, suggesting that melting can be triggered by different mechanisms, like grain boundary formation or defect unbinding. We find that the ratio of defects at the liquid-hexatic or liquid-coexistence phase transitions could determine the nature of these transitions and the mechanism underlying the melting process. The effect of the interaction of particles with their first- and second-nearest neighbors is also discussed.

I. INTRODUCTION

Melting in two dimensions (2D) has attracted attention through the last decades due to several factors: first of all, its controversial nature [1–5], but also the development of low dimensional devices and bidimensional materials with many potential applications such as graphene layers or carbon nanotubes [6–8], or the applications in the biological field, like the description of the crystallization and melting processes of bacteria colonies in a bidimensional model system [9].

Long-range positional ordering (also called translational ordering) cannot exist in bidimensional systems, while the orientational ordering is still possible at long distances, as it was first argued by Peierls [10] and Landau [11] and finally demonstrated by Mermin [12]. This fact has been observed both experimentally [13–16] and in simulations [1–5,17], showing that positional correlation decays algebraically, but the orientation can be maintained constant even for long distances, like in three-dimensional (3D) systems.

With the aim of understanding the phase transitions in these systems, the Kosterlitz, Thouless, Halperin, Nelson, and Young (KTHNY) theory [18–20] provides a theoretical explanation for 2D melting. It has been supported by several experiments performed on different systems: liquid crystals [21,22], atoms adsorbed on graphite surfaces [23,24] or in colloidal suspensions of charged particles [13] or particles with magnetic interaction [25,26], as well as by several simulations (see, e.g., Refs. [1–5]). In the framework of this theory, the evolution from the solid to the liquid state is produced through two continuous phase transitions. The first one is a transition from the solid to an intermediate phase, called hexatic, which has no analogy in 3D systems. This phase is characterized by an exponential decay of the positional ordering and an algebraic decay of the orientational ordering (in both cases vs distance). Thus, in this phase, the orientation has a quasi-long-range ordering, but the translational order is no longer maintained at large distances. The second phase transition occurs when orientational ordering is also destroyed, evolving from the hexatic to the liquid phase. In the liquid phase, both the orientational and positional ordering decay exponentially with the distance, so only short-range correlations can be observed.

Therefore, following the 2D KTHNY melting theory, transitions involved in the melting process are second-order or, equivalently, continuous transitions. Note that, in both transitions, the free energy shows a continuous behavior. The change between the solid and hexatic phase is second order because the correlation length of the translational order diverges in the solid phase, and the hexatic-liquid transition is also second order, as the correlation length of the orientational order diverges in the hexatic phase.

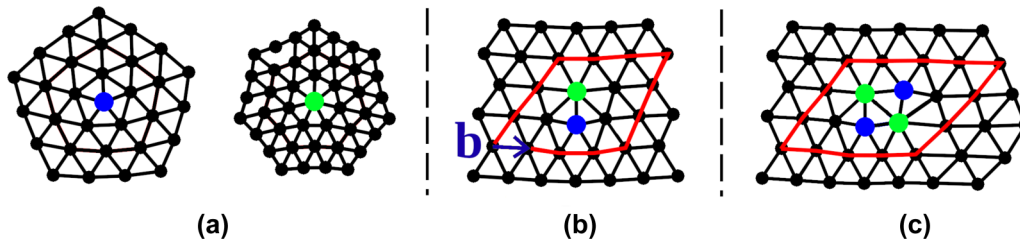*Corresponding author: otoledano@ccia.uned.es

FIG. 1. Schematic representation of different kinds of defects which can be present in a two-dimensional (2D) lattice. Particles with five and seven nearest neighbors are represented in blue and green, respectively. (a) Isolated disclinations with five and seven nearest neighbors on the left and right scheme, respectively. (b) Isolated dislocation, formed by two adjacent disclinations with five and seven nearest neighbors, respectively. Burgers vector of the dislocation is represented in blue. The closed trajectory corresponding to the perfect lattice is represented in red. (c) Dislocation pair, formed by two adjacent dislocations with opposite Burgers vectors (not shown). Its total Burgers vector is null, as the closed trajectory around the dislocation pair corresponding to the perfect lattice matches with that of the real lattice.

According to the KTHNY theory, these two transitions are due to the unbinding of topological defects. It relies on the assumption that the chemical potential of these defects is large enough to induce a low concentration of defects [18]. In fact, the model system of the KTHNY theory is a diluted gas of defects, so it could fail in reproducing phase transitions for systems with significant defect concentration [27].

Three different kinds of 2D defects can be considered: disclinations, dislocations, and dislocation pairs (see Fig. 1). In a 2D triangular lattice without defects, every particle has six nearest neighbors. A disclination is a topological defect composed of a single particle with coordination number different from six, typically five or seven [Fig. 1(a)]. This kind of defect affects both to the positional and the orientational ordering of the lattice and is defined by the defect charge, a scalar quantity which takes values of -1 and $+1$ for point defects with seven and five nearest neighbors, respectively. A dislocation is equivalent to a pair of disclinations, one with five and the other with seven nearest neighbors [see the case of adjacent disclinations in Fig. 1(b)]. This second kind of defect affects only the translational ordering, leaving almost unaltered the orientation of the lattice. Dislocations are defined by a vector quantity named the Burgers vector, which is the vector that completes a closed trajectory around the dislocation, taking as reference the closed trajectory found for a perfect lattice without defects (see Fig. 1). The third type of defect is the dislocation pair, which is composed of two adjacent dislocations with opposite Burgers vectors, so the total Burgers vector of a dislocation pair is null [see Fig. 1(c) in which the Burgers vectors are not present for this type of defect]. Thus, a closed trajectory around a defect which presents a null Burgers vector (as in a perfect lattice) will imply that the translational ordering is conserved for those kinds of defects, so this last kind of defect preserves not only the orientational but also the translational order. As the only kind of these three topological defects which preserves both types of ordering, the dislocation pair is the only which could be present in the solid phase with a representative concentration.

According to the KTHNY theory, as the temperature raises, the first phase transition occurs when these dislocation pairs found in the solid phase split into two isolated dislocations, losing the translational, but keeping the orientational ordering basically unaffected. That leads to the hexatic phase. Then

a second phase transition occurs when these isolated dislocations break into single disclinations, thus ruining both the positional and orientational organization, and the system becomes a liquid.

Within the KTHNY theory, defects mutually interact via a logarithmic potential, but they also add a contribution to the energy of the system (named core energy), due to the increase of energy produced by the distortion of the lattice in the neighborhood of these defects [18–20]. Thus, the Hamiltonian of the dislocations of the system will have two terms: the first of them represents the interaction energy between dislocations and the second the core energy of the dislocations. The interaction energy between dislocations depends on the position and the mutual orientations of the Burgers vectors of the interacting dislocations. On the other hand, the Hamiltonian corresponding to the disclination interaction is analogously described by two terms: the first corresponding to the interaction between disclinations and the second to the core energy of the disclinations. The interaction between disclinations depends on the position and their defect charge.

The interactions among defects being approximately canceled because they are distributed with different orientations to minimize their mutual interaction energy, the existence of defects is thus mainly influenced by the core energy of the different kinds of defects formed and by the temperature and concentration of the system. However, when the core energy becomes small enough, the concentration of defects can rapidly grow, leading to a scenario which cannot be fairly described by the KTHNY theory. In this situation, melting could be triggered by other mechanisms, and the Hamiltonians mentioned are no longer valid.

In addition to the KTHNY theory, a melting process involving the formation of grain boundaries was proposed by Fisher *et al.* [28] and revised by Chui [29,30] and has been observed in simulations with significant concentrations of defects [31]. According to the detailed studies of Chui [29,30], this melting process is characterized by the existence of a first-order transition between the hexatic and liquid phase (in contrast with the continuous transitions proposed in the framework of the KTHNY theory). These two theories for the 2D melting process have been tested in simulations in which the core energy of the defects was deliberately modified [31–33]. For large core energies, simulations show that

the melting process obtained was continuous, a situation that could be described by the KTHNY theory, whereas for small core energies the formation of grain boundaries of dislocations was the most plausible explication for the solid-liquid transition. The grain boundary theory described by Chui [30] also establishes a shift from a firm first-order transition from solid to liquid phase for high core energies to a weak first-order transition when the core energy of the dislocations is lower than $2.84 k_B T$ [30]. On the other hand, it has been observed experimentally that a quasi-2D colloidal system of hard spheres melts via a mixed scenario, where the hexatic-solid transition is continuous and the liquid-hexatic one is first order, showing a coexistence region [34].

Additionally, other melting mechanisms have been proposed, such as the simultaneous unbinding of dislocations and disclinations, which could occur when the binding energy of the disclination pairs is small, causing the rapid split of the disclination pairs after dislocation pairs are separated. This mechanism yields a single first-order transition between the solid and liquid phases, without the mediation of an intermediate hexatic phase [35,36].

Several computational studies have been performed to determine which of these hypothetical scenarios are obtained for different simulation conditions as the type of potential interaction or different temperatures and concentrations (see, e.g., Refs. [1–3,5,17,37–39]). All simulations confirm that, when the hexatic phase is present in the melting scenario of a particular system, it is always obtained via a continuous transition from the solid phase. However, the nature of the phase transition from the hexatic to liquid phase depends on both the potential energy function selected and the thermodynamic conditions of the system (temperatures and concentrations). It has been demonstrated that, for systems interacting by hard disc or repulsive disc potentials with a power law of $V \propto r^{-n}$ and $n > 6$, a first-order transition occurs from the hexatic to liquid phase [1]. Other potentials, like those with a soft repulsive component (soft-core potentials), show similar results for temperature or concentration ranges below certain critical values (T_c and ρ_c) [5]. In the case of repulsive potential functions with $n < 6$, this transition is found to be continuous [1], as for systems with soft core potentials and temperature and concentration values larger than T_c and ρ_c. In this power law repulsive system, density dominates the melting transition, as temperature has no role due to the lack of a potential energy scale. Simulations with the usual Lennard Jones (LJ) 6–12 potential have also been carried out [2], leading to similar conclusions to those using soft core potentials, and obtaining also analogous critical values of T_c and ρ_c. However, to the best of our knowledge, a systematic study of the influence of the shape (both the presence of an attractive region and its range) of the potential function has not been performed yet. In addition, a recent study has discussed the possible role of the attractive forces [40] which should also be explored.

In this paper, we will discuss the influence of the range of the interactions and the role of both the repulsive and the attractive part of the potential energy functions in the nature of these 2D phase transitions under different thermodynamic conditions, as it has not been clearly determined in previous works. The nature of the transitions from solid to hexatic and from hexatic to liquid phase will also be analyzed for representative cases. To achieve these purposes, we have performed Metropolis Monte Carlo (MMC) simulations with about 256^2 particles using the well-known LJ 6–12 and Morse potentials, which can be systematically tuned to vary the width of the potential (and consequently the range of the interaction) and the strength of the repulsive part. We will compare the values of the concentrations at which the liquid-hexatic transition takes place, for the full and truncated Morse potential function. With this objective, we will analyze the position of the neighbors in terms of the different regions of the selected potential energy function (i.e., the repulsive, attractive, or equilibrium regions) for the concentration range where the phase transition occurs. In addition, the possible mechanisms underlying the melting process obtained for the different thermodynamic conditions and interactions will be discussed, and the results will be compared with the existing theories. Also, the nature of the hexatic-liquid phase transition is discussed in terms of the ratio of defects.

II. METHODS

To carry out these simulations, we have developed a specific code [41]. It uses the MMC method to simulate a bidimensional system of particles in an NVT ensemble. A 2D simulation box with periodic boundary conditions and $N \simeq 256^2$ particles has been selected for the simulations. Changing the size of this simulation box allow us to use different particle concentrations, $\rho = N/S$, with S being the area of the box. This number of particles allows us to determine the long-range behavior of the translational and orientational correlation functions and to visualize the possible Mayer-Wood loop of coexistence [1,42]. For the desired concentration, a perfect triangular lattice was chosen for the initial configuration of the system, so the unit cell vectors a and b were orthogonal. We used a lattice which had 237×137 rectangular cells with two particles in each cell (the number of particles differs less than 1% from 256^2), one in the center and the other in the corner of the cell, distributed over a square simulation box, yielding a unit cell with $|a| = 0.999\sqrt{3}b$. This initial configuration was chosen because the melting process is performed much faster than the solidification process, as the range of the correlations in the solid phase is much larger than in the liquid one.

The trial movements of the MMC simulation were evaluated by selecting a randomly chosen distance and orientation, their values chosen with equal probability in the $[0,r_{max}]$ and $[0,2\pi]$ ranges, respectively, thus allowing detailed balance [43]. To accelerate the thermalization process and perform a more representative sampling, the maximum amplitude of the trial movements was set in such a way that the rejected and accepted movements were approximately the same [43]. Thermalization of the system should be achieved when the value of the global orientational order parameter of the system (see description below) is fluctuating around a constant value with no noticeable drift. The values of the amplitude of these fluctuations strongly depend on the system simulated, obtaining the largest values ~0.1 (for typical values of the order parameter ~0.3–0.5) for systems with coexistence between the hexatic and the liquid phases, and the lowest values of

$\sim 2 \times 10^{-3}$ for solid phase (with typical values for the order parameter ~ 0.7–0.9).

The global orientational order parameter is a vector defined as: $\vec{\Psi} = \frac{1}{N} \sum_{i=1}^{N} \vec{\psi_i}$, where $\vec{\psi_i}$ is the local orientational order parameter vector corresponding to the particle i. According to this definition, the direction of $\vec{\Psi}$ will define the global orientation of the system, and its module will take values between 1, for perfect oriented lattices, and 0, for nonoriented systems. In a 2D system with a triangular lattice arrangement, the local orientational parameter $\vec{\psi_i}$ of each particle is defined by

$$\vec{\psi_i} = \sum_{j=1}^{n_i} e^{6i\theta_{ij}}, \qquad (1)$$

where θ_{ij} is the angle formed by the vector $\vec{r_{ij}} = \vec{r_j} - \vec{r_i}$ (for particles i and j) and an arbitrary direction, which has been chosen to lay along the x axis, and n_i is the number of nearest neighbors of the particle i. The components of the $\vec{\psi_i}$ vector are the real and imaginary parts of Eq. (1), and its module will take a value of 1 when all the nearest neighbors are located, forming a perfect triangular lattice. The direction of this vector $\vec{\psi_i}$ will give us the local orientation of the nearest neighbors around particle i.

To decide which are the nearest neighbors of each particle, typically, two kinds of methods have been proposed for these studies [44]: the use of the Delauney graph (which is the dual graph of the Voronoi diagram) of the particles and the use of a cutoff radius, which is typically determined by the examination of the radial distribution function $g(r)$. In this paper, the second method has been employed, and only the pairs of particles separated a distance smaller than the first minimum of the $g(r)$ function were considered as nearest neighbors. The existence of a defect was considered when the number of the nearest neighbors of a particle was different than six.

The radial distribution function $g(r)$ was also used to analyze the translational ordering. As we were interested in the decay of the translational correlation with the distance, the behavior of this function was explored in only one direction, defined by the global orientational order parameter at each step. As different positional correlation patterns could be obtained depending on the chosen direction, we analyzed $g(r, 0)$ along the mentioned direction. In addition, and for the sake of clarity, the translational correlation function was redefined as $C(r, 0) = g(r, 0) - 1$, with zero value for noncorrelated distances, and positive values for correlated distances.

In addition, the local orientation correlation function, which is defined by Eq. (2), was also analyzed. Assuming a particle placed at the origin, the local orientational correlation at a distance r to that particle is given by

$$\eta(r) = \langle \vec{\psi_i} \cdot \vec{\psi_j} \, \delta(r - r_{ij}) \rangle, \qquad (2)$$

where $\delta(r - r_{ij})$ stands for the Dirac delta function of the distance between two particles r_{ij}. This correlation function will take the value 1 when the orientations of the particles at a distance r are parallel, and -1 for those distances at which particles orientations are antiparallel.

The decay rate of these correlation functions can be fairly analyzed in a logarithmic representation (see the insets of Fig. 2). If both axes (the correlation function value and the
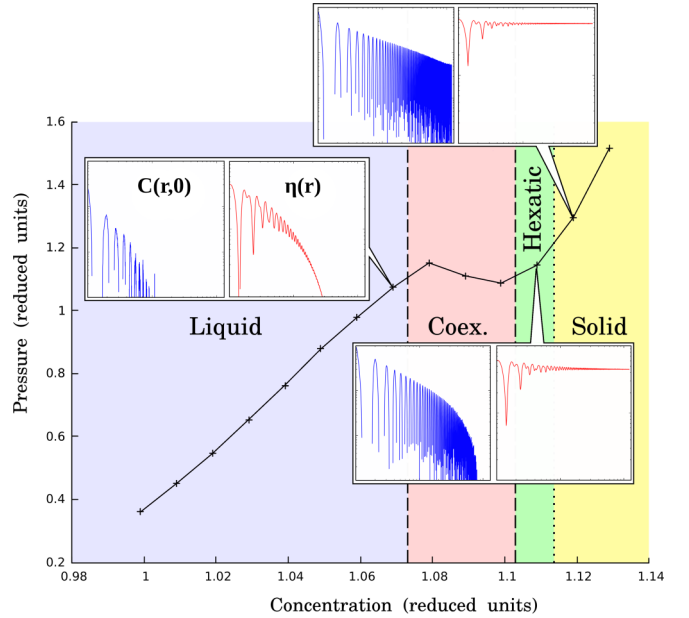

FIG. 2. Mayer-Wood loop of pressure vs concentration for a Morse potential with $\alpha = 5$ and $T = 0.5$. At the indicated points, the insets represent the translational $C(r, 0) = g(r, 0) - 1$ and orientational $\eta(r)$ correlation functions, in blue and red, respectively. Both axes (correlation function values vs distance in reduced units) in the insets are in logarithmic scale, so an algebraic decay of the correlation is visualized as a straight line with negative slope.

distance) are in logarithmic scale, an algebraic decay will be depicted as a straight line with a negative slope which defines the exponent of the decay [see $C(r, 0)$ in the solid phase of Fig. 2]. Otherwise, if the decay rate is exponential, correlation functions in the log-log scale will not fit to a straight line, and they rapidly fall down (as in the case of the liquid phase in Fig. 2).

Besides studying the decay of the correlation functions $C(r, 0)$ and $\eta(r)$, we can extract information about the nature of the phase transitions from the pressure vs concentration (P-V) curves. Pressure is computed from [43]

$$P = \rho k_B T + \frac{1}{2S} \sum_{i=1}^{N} \sum_{j>i}^{N} \vec{F}(r_{ij}) \cdot \vec{r}_{ij}, \qquad (3)$$

where S is the total area of the system, $\vec{F}(r_{ij})$ is the force between particles i and j, ρ is the particle concentration, and T the temperature of the system. For a continuous phase transition, pressure is revealed as a monotonically increasing function along the concentration [see Fig. 3(a)], while for a first-order phase transition, a Mayer-Wood loop must appear in the P-V curve [17,42] (see Fig. 2). The existence of this loop can only be explained by the interfacial tension effects of a phase coexistence in a finite system [42], as a characteristic imprint of a phase coexistence region. In addition, in the case of two phases with different densities, the analysis of the local density distribution can reveal the arising of a phase coexistence region.

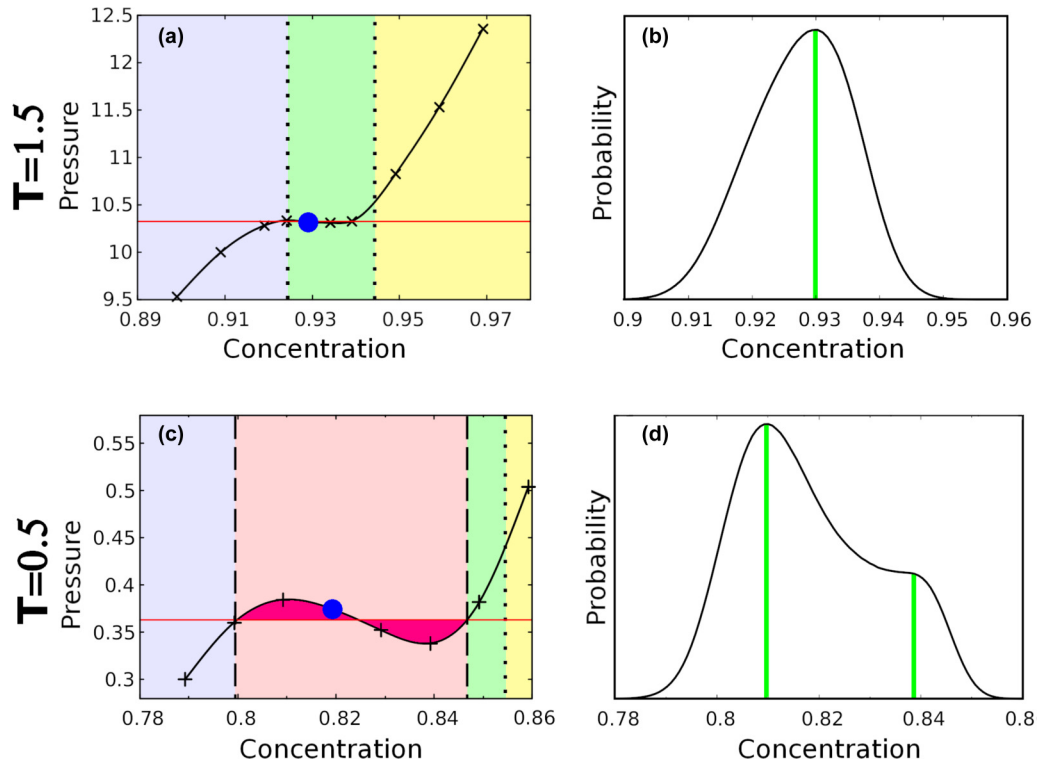To determine the region in which the phase transitions occur and their nature, we analyzed the P-V curves and

FIG. 3. (a) and (c) Pressure vs concentration curves at temperatures $T = 1.5$ and 0.5, respectively, in Lennard-Jones (LJ) reduced units, for a system of $N \simeq 256^2$ particles interacting via an LJ 6–12 potential. Red lines represent the pressure obtained from the Maxwell construction in panel (c) and the transition pressure in panel (a). Colors corresponding to the different phases are the same as in Fig. 2, and the areas resulting from the Maxwell construction in (c) are highlighted. In panels (b) and (d), the probability distribution function of the local densities obtained in the simulations performed for the concentration and temperature values marked with a blue point in panels (a) and (c), respectively, are shown.

the decay of the translational and orientational correlation functions. When no Mayer-Wood loop is observed on the *P-V* curve during a phase transition, the phase boundaries are specified uniquely by the rate of the decay of the positional and orientational correlation functions [1]. In return, if the Mayer-Wood loop exists for a certain temperature, the boundaries of the coexistence region are determined by the Maxwell construction [17] [see panel (c) in Fig. 3]. In this construction, a *P-V* diagram is depicted, and the first-order transition is characterized by a constant pressure value. This pressure value is selected to make the two areas delimited by this value equal in the *P-V* curve [see Fig. 3(c)]. The phase coexistence occurs in the region among the corresponding initial and final concentration values.

In this paper, two different potential functions are used to model the particle interaction: an LJ 6–12 and a Morse potential. We can define the potential interaction in the system by

$$V_{\text{eff}}(r) = V(r) - V(r_{\text{cut}}), \qquad (4)$$

where r_{cut} is the cutoff radius used for the potential energy calculation and $V(r)$ is modeled by $V^{\text{Morse}}(r) = D_e\{[1 - e^{-\alpha(r-\sigma)}]^2\}$ or $V^{\text{LJ}}(r) = 4D_e[(\frac{\sigma}{r})^{12} - (\frac{\sigma}{r})^6]$, which are the functions defining the Morse and LJ 6–12 potentials, respectively. In these expressions, σ is the equilibrium distance in the Morse potential or the distance at which the LJ potential becomes zero, D_e is the depth of the potential well, and

α the parameter that controls the width of the Morse potential well. The cutoff radius is selected so $V(r \in [r_{\text{cut}}, \infty)) < 10^{-3}D_e$, except for the simulations which retain only the repulsive part the of the Morse potential, where the cutoff radius is fixed to $r_{\text{cut}} = \sigma$. To compare the results obtained for different values of α, we have used the reduced units $\sigma = 1$, $D_e = 1$, and $k_B = 1$. Pressure is thus expressed in units of D_e/σ^2, and temperature is expressed in units of D_e. The range of temperatures in our simulations goes from $T = 0.5$ to 3.0.

III. RESULTS

In Subsec. A, we will review the phase transitions obtained with an LJ 6–12 potential at low and high temperatures, which have been recently studied by Hajibabaei and Kim [2]. Then in Subsec. B, we will discuss the nature of these transitions when particles interact via a Morse potential, varying the value of the potential parameter α. The influence of only considering the repulsive part of the Morse potential (caused by truncating the attractive part) will be examined in Subsec. C. Finally, in Subsec. D, the ratio of defects at the liquid-hexatic transition will be analyzed.

A. Lennard-Jones potential: A review

Phase transitions of bidimensional systems with LJ 6–12 potential have been recently studied by Hajibabaei and Kim [2] using the event-chain Monte Carlo algorithm [45]. In this
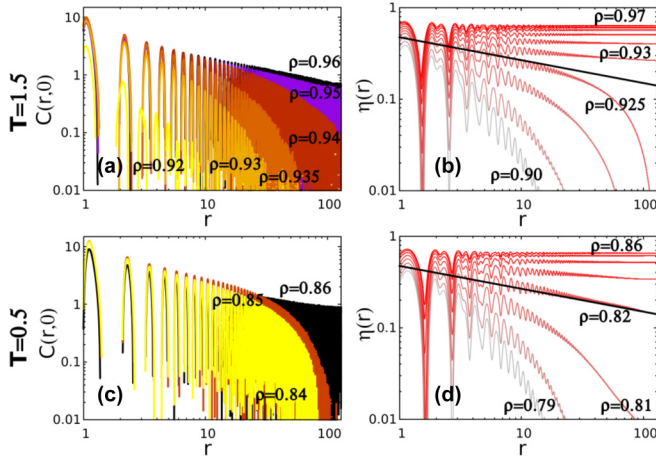
FIG. 4. Variation of the positional and orientational correlation functions $[C(r, 0)$ and $\eta(r)]$ along the distance in a system of particles interacting via a Lennard-Jones (LJ) 6–12 potential at temperatures $T = 0.5$ for (a) and (b) and $T = 1.5$ for (c) and (d). Double log axes are selected in both representations, so a straight line represents an algebraic behavior. In panels (b) and (d), the black lines represent an algebraic decay with exponent -0.25, corresponding to the expected behavior of the orientational correlation in the hexatic-liquid transition predicted by the KTHNY theory.

paper, we have performed an analogous simulation using the MMC method [41], and the results obtained in both cases are compared. The results of the LJ 6–12 simulation are used as a reference to evaluate the changes arising when the Morse potential is selected. Furthermore, this benchmark simulation helps to estimate the key computational parameters that should be carefully selected in the MMC method, as the number of steps needed to accomplish the thermalization process.

When particles interact under an LJ 6–12 potential function, the evolution from hexatic to liquid phase occurs via a first-order transition for temperatures lower than the critical temperature T_c or via a continuous phase transition for temperatures higher than T_c. This has been observed in previous simulation studies [2], where the critical temperature was determined to be around $T_c = 1.1$, in reduced LJ units.

Simulations of two representative cases have been carried out for temperatures below and over T_c, $T = 0.5$ and 1.5, respectively (see Fig. 3). Figure 3 shows that a Mayer-Wood loop of pressure is present for the phase transition occurring for temperatures below T_c, for $T = 0.5$ [panel (c)], but not when $T > T_c$, for $T = 1.5$ [panel (a)], as it was previously observed in Ref. [2]. This result confirms that the transition from hexatic to liquid phase can be classified as a first-order transition at $T = 0.5$ and as a continuous transition at $T = 1.5$.

For $T = 1.5$, the Mayer-Wood loop is not present [see Fig. 3(a)], so no phase-coexistence region is expected in this transition at this temperature. By inspection of the local density profile in the hexatic/liquid transition, a single maximum [see Fig. 3(b)] is observed, which supports this hypothesis. On the other hand, by inspection of the decay rate of the correlation functions $C(r, 0)$ and $\eta(r)$ at different concentration values [see panels (a) and (b) of Fig. 4], the phase transition concentration values can be directly estimated at this

temperature, $\rho_{\text{sol-hex}} = 0.945$ and $\rho_{\text{hex-liq}} = 0.927$, which are very close to those obtained in Ref. [2] $\rho_{\text{sol-hex}} = 0.938$ and $\rho_{\text{hex-liq}} = 0.926$.

When $T = 0.5$, by means of the inspection of the Maxwell construction [see Fig. 3(c)], we can also estimate that the range of concentration values for the coexistence region is approximately $\rho_{\text{coex}} \in (0.800, 0.847)$, which are very close to the range of values found with the event-chain simulation method $\rho_{\text{coex}} \in (0.810, 0.842)$ [2]. In addition, it can be observed in Fig. 3(d) that the local density profile is bimodal (it presents two peaks) in the coexistence region, which is in fact another hint of the coexistence of two well-differentiated phases at these thermodynamic conditions. Note how a small variation in the concentration value (from $\rho = 0.86$ to 0.85), triggers a noticeable qualitative change in the decay rate of the translational correlation function, $C(r, 0)$ [Fig. 4(c)]. This dramatic change corresponds to the solid/hexatic transition region. An approximately algebraic decay is obtained for a concentration of $\rho = 0.86$, corresponding to the expected behavior in the solid phase, but for slightly lower concentration values (just for $\rho = 0.85$), the trend of the translational correlation function can be now fitted to an exponential decay, which is related to a short-range positional order. However, in panel (d) of Fig. 4, it can be noted that the orientational order is lost at lower concentrations (below $\rho = 0.82$), so there is a narrow region where translational order is absent while the orientational order is preserved (between $\rho = 0.82$ and 0.85), indicating the existence of a hexatic phase in this transition. It can also be appreciated in panel (b) of Fig. 4 that the transition from an algebraic to an exponential decay of the orientational order appears when the exponent of the algebraic decay is approximately -0.25, as predicted by the KTHNY theory. At this temperature ($T = 0.5$), the obtained concentration value for the transition from hexatic to solid phase, where the translational correlation undergoes a drastic change for long distances, is about $\rho_{\text{sol-hex}} = 0.855$ [see panel (c) of Fig. 4]. This result is also very similar to that found in previous studies $\rho_{\text{sol-hex}} = 0.848$ [2].

Finally, we would like to mention that the thermalization of the system was achieved after a maximum of 10^7 MMC steps for all simulations, where each step consists of a trial movement on each particle. When we choose concentration-temperature values far from the phase transition points (for solid and liquid phases), the thermalization is achieved almost instantaneously, but when regions near the transition points or in the coexistence interval are explored, this process required much larger computational times.

B. Full Morse potential

In this section, we present the results obtained when the Morse potential is selected. We will use different values of the parameter α, which controls the width of the potential well. Previous simulations were performed in the NPT ensemble within the molecular dynamic approximation [39]. This paper completes those previous analyses by performing simulations within the NVT ensemble in larger systems, thus reducing finite size effects. We have followed a procedure like that used for the LJ 6–12 potential, but now the particles interact
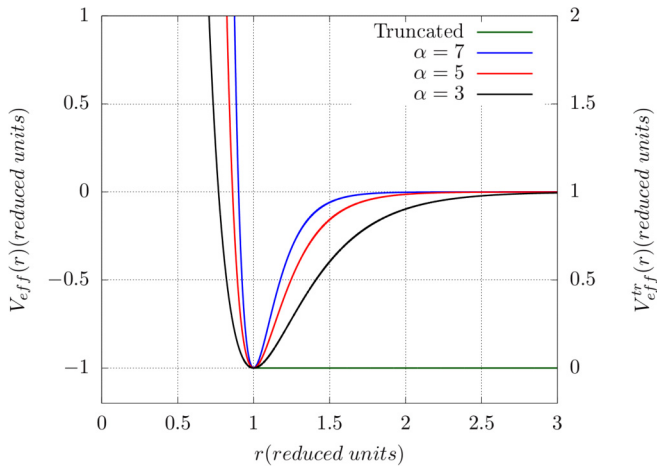
FIG. 5. Potential energy functions modeled by full and truncated Morse potentials [see Eq. (4)] for different values of the α parameter, where the energy scales for the full V_{eff} and truncated $V_{\mathrm{eff}}^{\mathrm{tr}}$ potentials are represented in the left and right axes, respectively.

through a Morse potential, with the following values of the α parameter: $\alpha = 3$, 5, and 7 (see Fig. 5).

As it can be seen in Fig. 5, smaller values of α yield a longer range of interaction and softer repulsive potentials, while the opposite occurs for higher values of α, which give potentials with a harder repulsion component and shorter ranges of attractive interaction.

By simple inspection of the *P-V* results depicted in Fig. 6, it can be observed that, for $\alpha = 3$, the Mayer-Wood loop is absent even at the lowest temperature of the simulation $T = 0.5$. Consequently, the transition between the solid and the hexatic phases is expected to be continuous for temperatures >0.5 when this soft-core and long-range potential function is acting. No further simulations at higher temperatures were carried out. For the other values of α, phase transitions for three different temperatures have been simulated (see Fig. 6). Larger values of α yield higher critical temperature T_c values because of the persistence of the Mayer-Wood loop for higher temperatures. In addition, for the same temperature values, consistently wider coexistence regions $\rho_{\mathrm{coex}} \in (\rho_{\mathrm{liq}}, \rho_{\mathrm{hex}})$ are
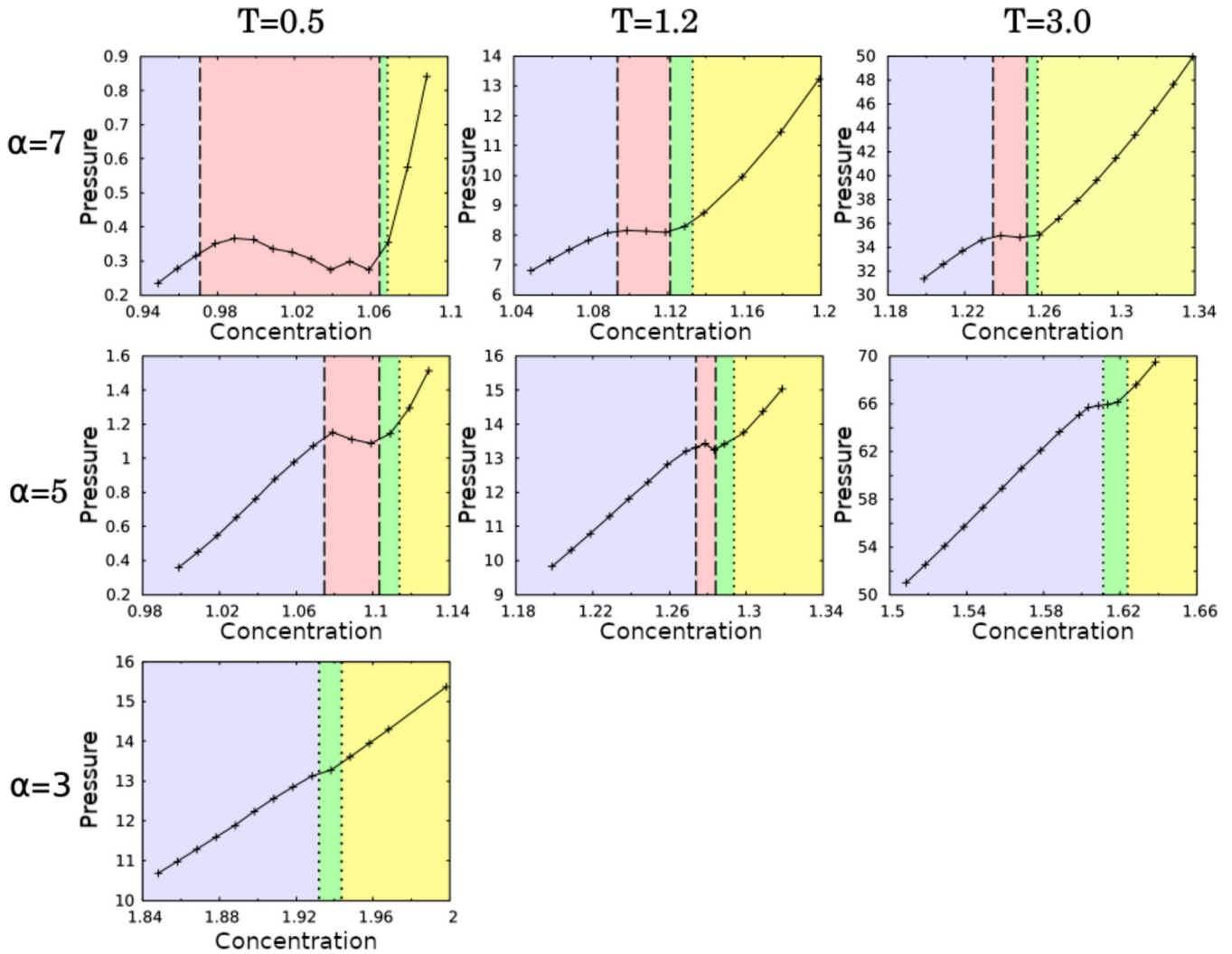

FIG. 6. Variation of pressure along the concentration for different values of α and temperature for a Morse potential. Concentration boundaries for each phase are marked with discontinuous or dotted lines for first-order or continuous transitions, respectively. Liquid, coexistence, hexatic, and solid phases are colored in blue, pink, green, and yellow, respectively.
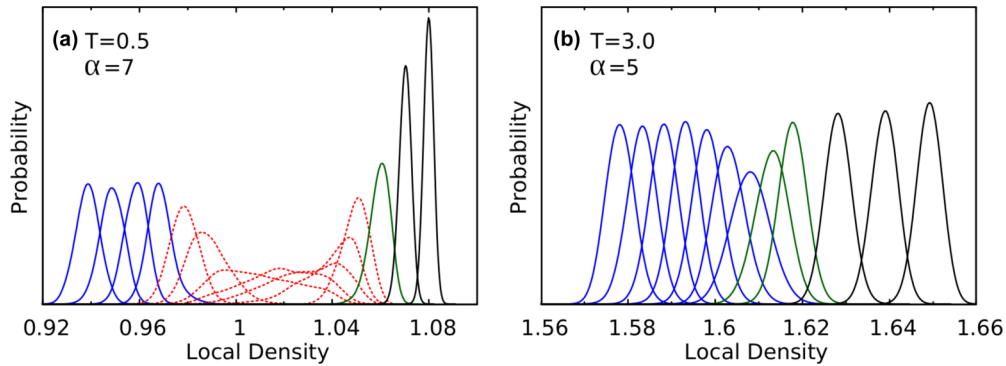
FIG. 7. Local density distributions in the phase transitions from liquid to hexatic phase for particles interacting via a Morse potential with $\alpha = 7$ at $T = 0.5$ and $\alpha = 5$ at $T = 3.0$ in panels (a) and (b), respectively. The liquid, hexatic, and solid phases are depicted with solid blue, green, and black lines, respectively, and phase coexistence is represented by the dotted red curve.

found for larger values of α (see Fig. 6). As shown in Fig. 7, the curve profiles of the local density distribution support also the existence of a coexistence region when the Mayer-Wood loop is present, showing a single peak distribution for those concentration-temperature values in which no Mayer-Wood loop is found, whereas several peaks appear for values inside the range of the coexistence region, in which a Mayer-Wood loop is obtained. In the curves of the local density distribution shown in Fig. 7(a), we observe that, within the range of concentrations where the system presents phase coexistence [$\rho \in (0.97, 1.06)$], a strong broadening of local density distribution is obtained. That reveals an existence of areas with a notable difference in the local density values. On the contrary, in Fig. 7(b), we can see how, in the vicinity of the phase transition between the liquid and hexatic phases, these curves undergo only a small broadening, showing that a more uniform local density distribution is achieved.

The translational and orientational correlation functions (see Fig. 8) are very similar to those of the LJ 6–12 potential (see Fig. 4), revealing that the hexatic phase is always found in all temperatures explored. Again, in agreement with the predictions of the KTHNY theory, the transition from the hexatic to the liquid phase is obtained when the exponent of the algebraic decay is around -0.25 [see panel (b) of Fig. 8]. It can be also remarked that, for values of α for which a

coexistence region between hexatic and liquid phases exits (i.e., for $\alpha = 5$ and 7), this region occupies a larger concentration range at lower temperatures (see discussion below).

C. Repulsive Morse potential

To understand the influence in the melting process of each part of the Morse potential function, both the attractive tail and the repulsive region, we have performed simulations for the same temperatures and α values as in the previous sections but using only the repulsive part of the potential function, which is equivalent to fix the cutoff radius value at $r_{\mathrm{cut}} = \sigma = 1$ in Eq. (4).

The phase transitions have been studied by analyzing the decay of the correlation functions. A notable result obtained in these simulations is that the Mayer-Wood loop of pressure is absent for all α and temperature values, as shown in Fig. 9. Consequently, when we only use the repulsive part of the Morse potential, and for the temperature values explored, the melting process is consistent with the KTHNY scenario, and it is mediated by two continuous phase transitions.

Figure 9 also indicates that, for the same temperature, the phase transition regions appear now at different concentration values with respect to those obtained with the full Morse potential function (Fig. 6). These shifts of the concentration
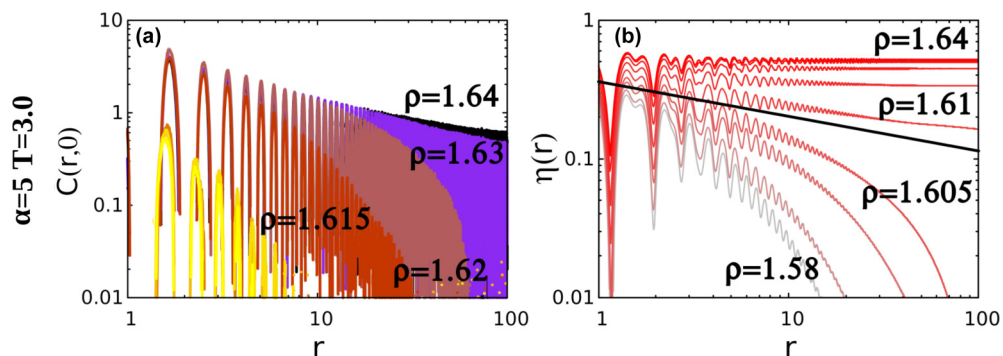

FIG. 8. Variation of the translational and orientational correlation functions $C(r, 0)$ and $\eta(r)$ along the distance in panels (a) and (b), respectively. Simulations were carried out with a full Morse potential with $\alpha = 5$ and temperature $T = 3.0$. Black solid line in panel (b) represents an algebraic decay with exponent -0.25, corresponding to the expected behavior in the hexatic-liquid transition in the framework of the KTHNY theory.
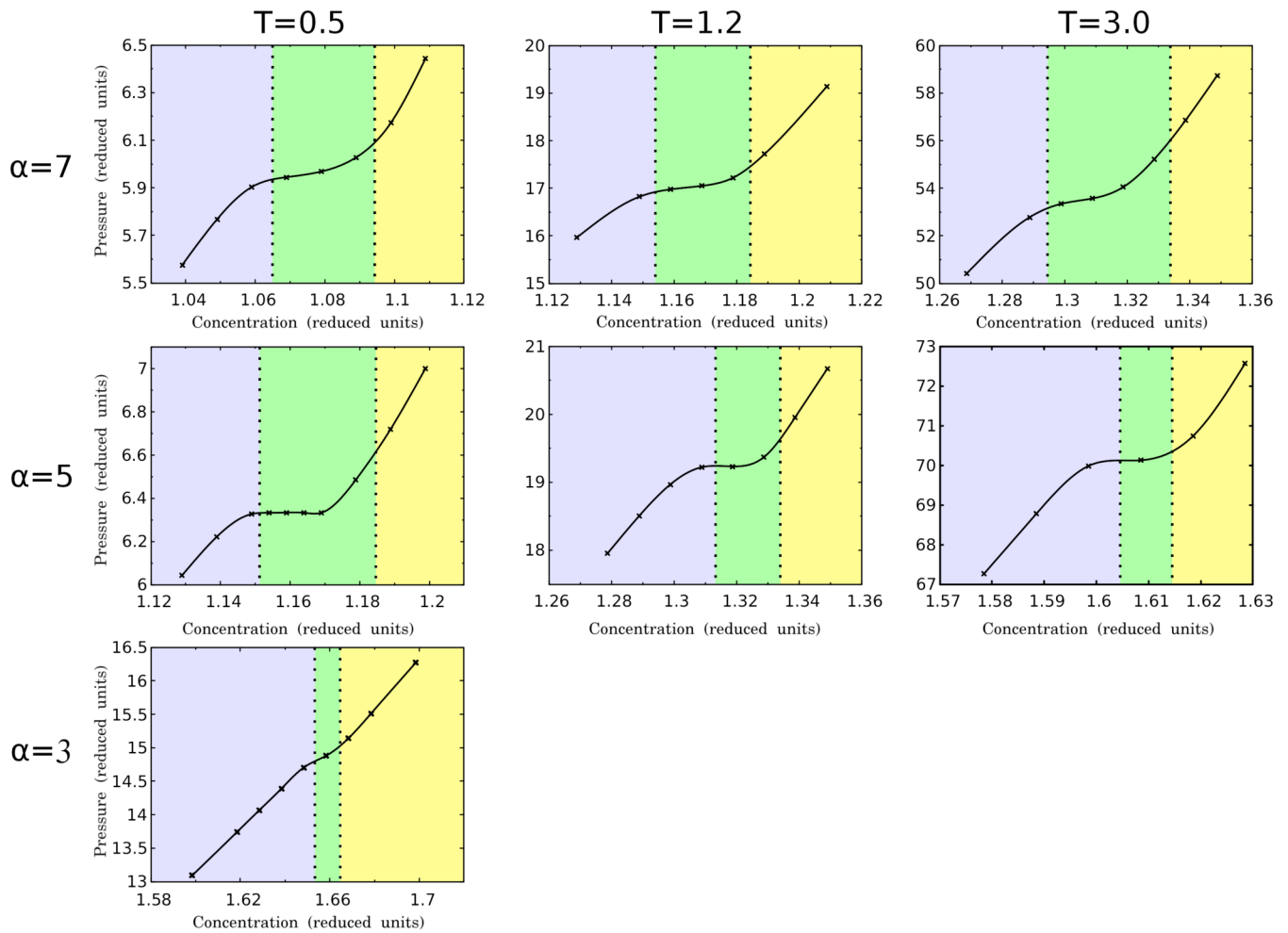
FIG. 9. Pressure vs concentration curves obtained for different α and temperature values for a system of particles interacting with only the repulsive part of the Morse potential function. The colors of the different phases are the same as in Fig. 6.

where the phase transition occurs can be to higher or lower values (see the Discussion section below).

D. Ratio of defects

The ratio of defects, which can be defined as the number of defects divided by the total number of particles N, has arisen in our simulations as a key parameter during the phase transition and could indicate which mechanisms are triggering the melting process (e.g., KTHNY, which assumes a low defect concentration, or the grain boundary theory, which is still suitable for a wider range of defect concentration). We plot in Fig. 10 the ratio of defects obtained in the liquid-hexatic transition for a given temperature.

A high ratio of defects yields first-order transitions (e.g., for $\alpha = 7$ for the full Morse potential, black line in Fig. 10), while the transitions become continuous for low enough ratio of defects (e.g., the case of $\alpha = 5$ for the truncated Morse potential, the orange line in Fig. 10). The critical defect concentration value between continuous and first-order transitions can be established at ~ 0.2, as can be appreciated in Fig. 10. Transitions at $T = 0.5$ and $\alpha = 3$ (results not shown) lead also to values of the ratio of defects values < 0.2, in concordance with the previous observation. In addition, the

coexistence region becomes wider when higher ratios of defects are obtained (e.g., at $T = 0.5$ and $\alpha = 5$ or 7 for the full Morse potential), indicating a stronger first-order transition.
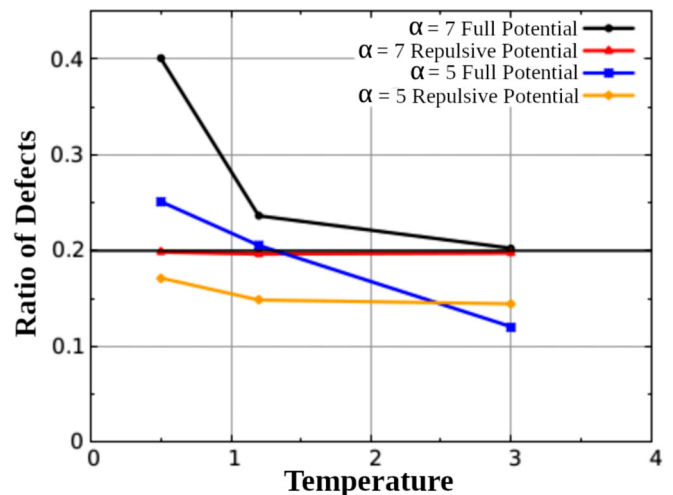

FIG. 10. Ratio of defects obtained in the phase transition from liquid to hexatic phase.

On the other hand, transitions occurring at values of ratios of defects slightly >0.2 ($T = 3.0$ and $\alpha = 7$ for the full Morse potential), show a weak first-order behavior, with narrower coexistence regions.

IV. DISCUSSION

Three aspects of the results of our simulations are now presented. First, we will discuss the two different melting processes obtained depending on the thermodynamic conditions and the potential functions selected. Then differences between the results obtained with the full and truncated Morse potential will be analyzed. We tried to elucidate which are the mechanisms underlying the different melting processes and why they depend on the system conditions and on the particle interaction function.

A. Continuous and first-order transitions

Two different kinds of melting processes have been obtained in our simulations, which could include first-order or continuous transitions. However, both processes always involve the existence of a hexatic phase, observed between the solid and liquid phases. The transition from the solid to the hexatic phase is always continuous for all the potential functions that we have employed (LJ 6–12, full Morse, and repulsive Morse potentials). The existence of this hexatic phase is supported by the fact that, in a small range of densities between the solid and the liquid phases (where the hexatic phase takes place), orientational correlation functions decay algebraically along the distance, while translational correlation functions decay exponentially. In the liquid phase, both orientational and translational correlation functions decay exponentially, and in the solid phase, a long-range orientational correlation and an algebraic decay in the translational correlation is observed (see Fig. 1). The absence of a Mayer-Wood loop of pressure in the vicinity of the concentration range of the transition from the solid to the hexatic phase supports the conclusion that this transition is always continuous. Furthermore, the local density distributions appear to always be unimodal in the range of concentrations around this transition point, so no phase coexistence is expected.

However, as observed in previous works [1,2], we obtain that transitions between the hexatic and liquid phases are first order in some cases and continuous in others, depending on the potential function and thermodynamic conditions selected in the simulation. This can be extracted by inspection of the evolution of the *P-V* curves at selected temperatures (Figs. 3 and 6).

When the LJ 6–12 potential is acting, a Mayer-Wood loop of pressure is obtained for low temperatures and concentrations (Fig. 3), indicating the existence of a first-order transition with a region of coexistence of both phases. For high temperature and concentration values, this loop vanishes, suggesting a mechanism that includes a continuous phase transition. These results, which agree with those of Ref. [2], have been recently questioned [40], arguing that, for repulsive discs with a potential energy function $V(r) = r^{-12}$, it has been previously demonstrated that the hexatic-liquid transition is first order [1]. However, if we compare the potential function
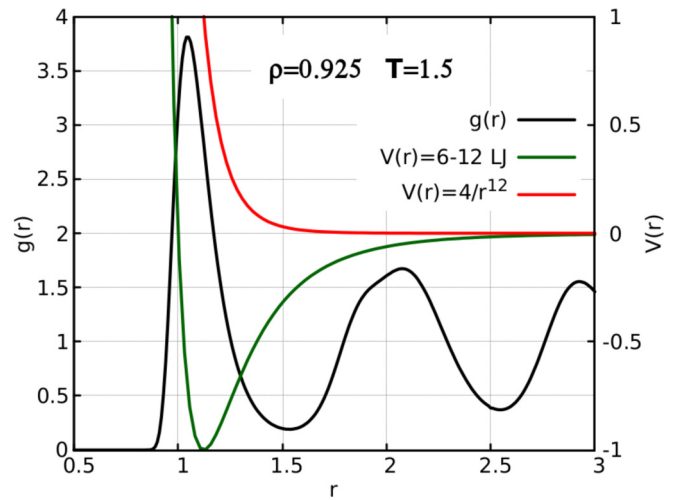

FIG. 11. The radial distribution function $g(r)$ obtained for the Lennard-Jones (LJ) 6–12 potential at $T = 1.5$ and $\rho = 0.925$ is plotted together with the LJ 6–12 potential energy function in reduced LJ units. The repulsive part of the LJ 6–12 potential energy function $V(r) = 4r^{-12}$ is also represented.

shape of the full LJ 6–12 potential with that of the repulsive r^{-12} part of this potential (see Fig. 11), in the region where the first neighbors are more probably found (for $T = 1.5$ and $\rho = 0.925$), both potential energy function shapes are very different. For much higher temperatures, where the melting process is obtained at lower concentrations, the effect of the attractive part of the potential could be disregarded, but this is far from being achieved in the range we have studied.

An analogous result is observed (see Fig. 6) for the full Morse potential when the value of α is large enough ($\alpha \geqslant 5$), i.e., for short-ranged interactions and hard-core potentials. A first-order transition from hexatic to liquid phases is observed at low concentration and temperature values, whereas a continuous transition appears for larger concentrations and temperatures. In this case, the concentration range of the coexistence region becomes smaller when the temperature is raised. For temperatures larger than a certain T_c, this region completely disappears, and the melting process becomes continuous. The observed value of T_c is lower for smaller α values, which causes that the melting process becomes continuous even at very low temperatures for low enough α values, i.e., for long-ranged interactions and soft-core potentials (see Fig. 6). When the Morse potential is truncated, the simulations reveal that the Mayer-Wood loop of pressure is absent for all values explored (see Fig. 9), so the melting process occurs always by a continuous transition in these cases.

B. Role of first and second-nearest neighbors in the melting process

Three different trends can be extracted by observing the changes in the concentration values where the phase transition (from liquid to hexatic or liquid to coexistence) takes place for the full and truncated Morse potentials. When our simulations are performed with the full Morse potential and the results reveal phase transitions occurring at low concentration values, equivalent simulations, but using the truncated potential,
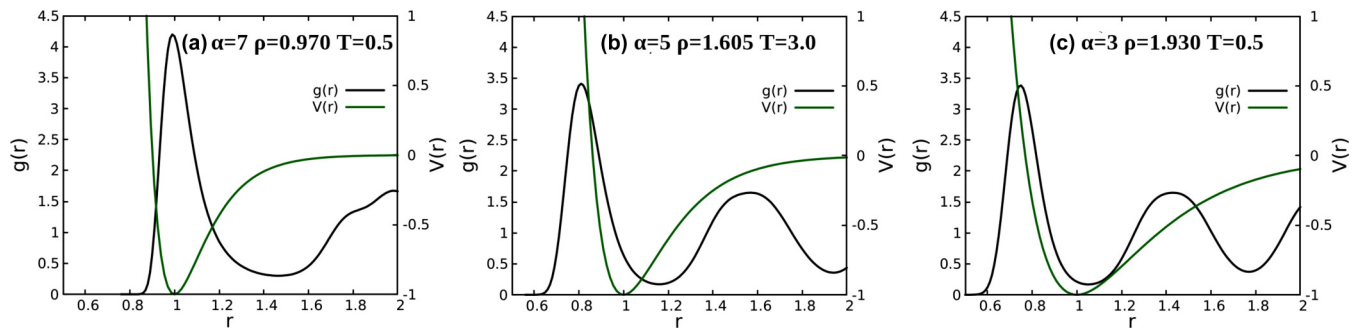
FIG. 12. The radial distribution function $g(r)$ obtained for different Morse potential energy functions $V_{\text{eff}}(r)$ and thermodynamic conditions is represented along the distance with the potential energy function selected. In panel (a), a low concentration system with $\rho = 0.97$ is depicted, where the distance of the first peak, corresponding to the nearest neighbors, coincides with the potential energy minimum. In panel (b), the radial distribution function of a system with intermediate concentration $\rho = 1.605$ is depicted, where the nearest neighbors lay in the repulsion part of the potential. In panel (c), which corresponds to the radial distribution function of a system with high concentration $\rho = 1.93$, we can see that, again, the nearest neighbors lay in the repulsive part of the potential, but now the second-nearest neighbors are located in a region with a still attractive enough part of the potential, which leads to forces which cannot be neglected.

yield phase transitions at higher concentration values. On the contrary, when the simulations using the full Morse yield high concentration values for the liquid-hexatic transition, the concentrations obtained for the truncated Morse remain at similar or even lower values.

When the liquid-hexatic transition occurs at low concentration values ($\sim$1.0–1.3), the distance between nearest neighbors is quite close to the position of the minimum of the energy potential function [see Fig. 12(a)], and the transition point obtained with the truncated potential is shifted to higher concentrations. This can be explained by the fact that the full Morse potential leads to more ordered systems, as the first neighbors are mostly confined in the potential well [see Fig. 12(a)], being necessary to perform a larger decompression to melt the hexatic.

If we analyze systems in which the liquid-hexatic transition occurs at high density values, the nearest neighbors are no longer in the region of the energy minimum of the potential function (in fact they are in the repulsive region of the potential). In these cases, for the truncated Morse potential, similar or even lower concentration values at the transition are obtained, compared with those with the full Morse potential. This can be explained by analyzing the position of the nearest and second-nearest neighbors. At high concentrations, the nearest neighbors are located in the repulsive region of the Morse potential [see Figs. 12(b) and 12(c)], leading to equivalent interactions between nearest neighbors for the full and truncated potentials.

However, now the interaction with the second-nearest neighbors can play a crucial role in the melting process, as they are placed at distances for which the resulting interaction is no longer negligible [see Fig. 12(c) where $\alpha = 3$ and $T = 0.5$]. Notice that the interactions with second-nearest neighbors occur in a direction different than those with the nearest neighbors, so they may cause a destabilization in the system. Therefore, these interactions (and the associated destabilization) occur only in the case of the full Morse potential, and the phase transitions for the truncated potential will require a further decompression than that yielded with the full potential, as shown by the simulations.

In addition, there are intermediate cases in which the concentration values at the transitions are similar in both the full and truncated Morse potentials. This occurs for α and concentration values for which the first neighbors are no longer in the minimum energy of the potential and the second-nearest neighbors do not play a significant role [see Fig. 12(b)]. This situation occurs for intermediate values of the α parameter, with a shorter range in the attraction tail and with harder repulsion, as in the case for $\alpha = 5$ and $T = 3.0$.

C. Defects: core energies and ratio of defects

For the LJ 6–12 and full Morse potentials, two different scenarios for the liquid-hexatic transition are obtained: we find a first-order (or a continuous) transition when concentration is below (or above) a certain critical value. The first scenario can be associated with the melting caused by the grain boundary formation, as the phase transition from hexatic to liquid obtained by this mechanism is discontinuous. The second scenario could be explained by the KTHNY theory, which predicts a continuous transition between hexatic and liquid phases.

As grain boundary theory applies when a high concentration of defects is present, they might occur in systems where the core energy of the defects is low enough and defects will be ubiquitous. For systems with low particle concentration, we expect to have lower core energies, enabling the emergence of many defects which could merge to form grain boundaries, and thus finally leading to first-order transitions.

For systems with a larger core energy for the defects, its number will be scarcer, and a model based on a diluted gas of defects (as is implied in the KTHNY theory) should be more appropriate to describe this situation. For systems with higher particle concentrations, higher defect core energies should be expected, disabling its massive production, and thus inhibiting the formation of grain boundaries. In this case, a theory based on a diluted gas of defects could be appropriate to describe the system, in which a continuous transition should be observed, in agreement with the KTHNY melting mechanism. Consequently, the core energy of the defects could determine the nature of the melting process.

This hypothesis is supported by the values of the ratio of defects obtained in our simulations around the liquid-hexatic or liquid-coexistence transition. When the transition takes place at high values of the ratio of defects, it has been observed that it is always first order, while continuous transitions have been obtained when this ratio is smaller at the transition point. The critical value of the ratio of defects, which separates the first-order and the continuous transitions, has been estimated to be ∼0.2 for the kind of systems studied (see Fig. 10). This critical value could depend on the potential shape and deserves to be studied in further works.

This analysis is also consistent with the absence of the Mayer-Wood loop in the simulations performed with the truncated Morse potential, as the maximum concentration values at which the pure liquid phase is observed (for given temperature and α) are larger than those obtained with the full Morse potential, thus producing an increase in the defect core energy and a subsequent decrease in the ratio of defects (always <0.2). On the other hand, previous simulations performed with repulsive discs acting with power law potentials give a continuous hexatic to liquid phase transition for high concentration values, while it turns discontinuous when the transition is produced at smaller ones [1].

Also, we want to highlight that when nonequilibrium molecular dynamics (NEMD) simulations [46,47] are used to describe the melting process induced by mechanical effects, such as shear and stress, the same sequence of phases (solid-hexatic-hexatic/liquid coexistence-liquid) as those obtained in our simulations in the low concentration regime is found. In these NEMD simulations, shear induces the formation of grain boundaries, and consequently, mechanical-induced 2D melting follows similar mechanisms to those yielded by thermal effects for low concentrations.

V. CONCLUSIONS

Our results of the MMC simulations carried out with the LJ 6–12 potential are in very good agreement with those previously obtained with the event-chain method [2]. Discrepancies between our results obtained with the LJ 6–12 potential and those previously obtained with the repulsive discs modeled by the power law potential $V(r) \propto r^{-12}$ [2] are explained in terms of the difference between both potential shapes in the region where the first neighbors are more probably placed.

In our simulations, we have always obtained a continuous liquid-hexatic transition when using the repulsive Morse potential. If the full Morse potential is employed (i.e., including the attractive part), this phase transition could become first order. If the value of α is decreased for constant temperature values, the coexistence region, if present, becomes narrower and finally disappears. The repulsive part of the potential becomes harder for larger α values and yields less concentrated systems at the transition point. For these low concentrations, the number of defects increases, so grain boundaries could be more easily formed.

Moreover, in the case of the full Morse potential, we have shown the relevant role of both the nearest and second-nearest neighbors in the concentration values at which the liquid-hexatic transition appears. These shifts in the concentration

where this transition takes place can trigger the change in the main mechanism of the melting process. As an example, we have found that, when removing the attractive part of the potential, the transition can turn from first order to continuous. This change can be explained by this shift in the concentration at the phase transition point. According to the results obtained in Ref. [2], we have observed that the introduction of an attractive potential well can induce a change from a continuous to a first-order transition. We have also shown the important effect of considering the second-nearest neighbors, as they can induce a destabilization of the system, which possibly gives light for understanding the transition for long-ranged attractive potentials.

In our simulations, an hexatic phase is always obtained in the melting process, so a hypothetical melting mechanism involving a simultaneous dissociation of both dislocation and disclination pairs can be disregarded. On the other hand, both theories, KTHNY and the grain boundary formation, are needed to explain the two different kinds of transitions observed in our results.

We have found that the ratio of defects can be responsible for triggering the different mechanisms underlying the transition. Systems with low particle concentration, with lower defect core energies, and many defects which could form grain boundaries, lead to first-order hexatic-liquid transitions. Systems with high particle concentrations will have a small ratio of defects, which could not form grain boundaries and a diluted gas of defects could describe the system, leading to continuous hexatic-liquid transitions, in agreement with the KTHNY theory. Moreover, we have characterized a critical ratio of defects ∼0.2 to obtain whether the liquid-hexatic transition is continuous or first order for defect ratios below or above that critical value, respectively. On the other hand, when the particle concentration at this transition shifts to higher values, the ratio of defects is found to decrease, yielding a narrower coexistence region.

In addition, our hypothesis could be compared favorably with experiments which characterize the freezing transition of monolayers of xenon adsorbed on a graphite substrate [24]. A first-order transition was observed for low coverages of 0.84–0.86 monolayers of xenon atoms, while it became a continuous transition when the coverage was augmented to about 1 monolayer. Low coverages can be associated with the low concentration scenario of our simulations, while the high coverage of about 1 monolayer could correspond to the high concentration scenario.

We conclude that the concentration of the system at the transition seems to be the main factor which determines the mechanism of the melting process. Excluding the hard discs potentials, for which temperature is irrelevant, the concentration at which the transition occurs always increases when the temperature is raised. Consequently, the melting mechanism changes from the grain boundary formation to a KTHNY-like melting. This dependence on the concentration can be ascribed to the change in the core energy of the defects formed in the system, as higher (lower) particle concentrations lead to higher (lower) core energies and lower (higher) ratio of defects, and a continuous (first order) hexatic-liquid phase transition is expected.

[1] S. C. Kapfer and W. Krauth, Two-Dimensional Melting: From Liquid-Hexatic Coexistence to Continuous Transitions, Phys. Rev. Lett. **114**, 035702 (2015).

[2] A. Hajibabaei and K. S. Kim, First-order and continuous melting transitions in two-dimensional Lennard-Jones systems and repulsive disks, Phys. Rev. E **99**, 022145 (2019).

[3] W. Qi, A. P. Gantapara, and M. Dijkstra, Two-stage melting induced by dislocations and grain boundaries in monolayers of hard spheres, Soft Matter **10**, 5449 (2014).

[4] J. Russo and N. B. Wilding, Disappearance of the Hexatic Phase in a Binary Mixture of Hard Disks, Phys. Rev. Lett. **119**, 115702 (2017).

[5] M. Zu, J. Liu, H. Tong, and N. Xu, Density Affects the Nature of the Hexatic-Liquid Transition in Two-Dimensional Melting of Soft-Core Systems, Phys. Rev. Lett. **117**, 085702 (2016).

[6] A. K. Geim and K. S. Novoselov, The rise of graphene, Nat. Mater. **6**, 183 (2007).

[7] K. S. Novoselov, V. I. Fal'ko, L. Colombo, P. R. Gellert, M. G. Schwab, and K. Kim, A roadmap for graphene, Nature **490**, 192 (2012).

[8] J. Meng, C. Niu, L. Xu, J. Li, X. Liu, X. Wang, Y. Wu, X. Xu, W. Chen, Q. Li, Zi. Zhu, D. Zhao, and L. Mai, General oriented formation of carbon nanotubes from metal-organic frameworks, J. Am. Chem. Soc. **139**, 8212 (2017).

[9] F. Ramos, C. López, E. Hernández-García, and M. A. Muñoz, Crystallization and melting of bacteria colonies and Brownian bugs, Phys. Rev. E **77**, 021102 (2008).

[10] R. E. Peierls, Remarks on transition temperatures, Helv. Phys. Acta **7**, 81 (1934).

[11] L. D. Landau, Theory of phase transformations, Phys. Z. Sowjet., **11**, 26 (1937).

[12] N. D. Mermin, Crystalline order in two dimensions, Phys. Rev. **176**, 250 (1968).

[13] C. A. Murray and D. H. VanWinkle, Experimental Observation of Two-Stage Melting in a Classical Two-Dimensional Screened Coulomb System, Phys. Rev. Lett. **58**, 1200(1987).

[14] G. E. Stein, E. J. Kramer, X. Li, and J. Wang, Single-Crystal Diffraction from Two-Dimensional Block Copolymer Arrays, Phys. Rev. Lett. **98**, 086101 (2007).

[15] T. Osawa, T. Kajitani, D. Hashizume, H. Ohsumi, S. Sasaki, M. Takata, Y. Koizumi, A. Saeki, S. Seki, T. Fukushima, and T. Aida, Wide-range 2D lattice correlation unveiled for columnarly assembled triphenylene hexacarboxylic esters, Angew. Chem. Int. Ed. Engl. **51**, 7990 (2012).

[16] S. Zamir, R. Poupko, Z. Luz, B. Hüser, C. Boeffel, and H. Zimmermann, Molecular ordering and dynamics in the columnar mesophase of a new dimeric discotic liquid crystal as studied by x-ray diffraction and deuterium NMR, J. Am. Chem. Soc. **116**, 1973 (1994).

[17] E. P. Bernard and W. Krauth, Two-Step Melting in Two Dimensions: First-Order Liquid-Hexatic Transition, Phys. Rev. Lett. **107**, 155704 (2011).

[18] J. M. Kosterlitz and D. J. Thouless, Ordering, metastability and phase transitions in two-dimensional systems, J. Phys. C: Solid State Physics **6**, 1181 (1973).

[19] D. R. Nelson and B. I. Halperin, Dislocation-mediated melting in two dimensions, Phys. Rev. B **19**, 2457 (1979).

[20] A. P. Young, Melting and the vector Coulomb gas in two dimensions, Phys. Rev. B **19**, 1855 (1979).

[21] J. Collett, P. S. Pershan, E. B. Sirota, and L. B. Sorensen, Synchrotron X-Ray Study of the Thickness Dependence of the Phase Diagram of Thin Liquid-Crystal Films, Phys. Rev. Lett. **52**, 356 (1984).

[22] E. B. Sirota, P. S. Pershan, L. B. Sorensen, and J. Collett, X-Ray Studies of Tilted Hexatic Phases in Thin Liquid-Crystal Films, Phys. Rev. Lett. **55**, 2039 (1985).

[23] J. P. McTague, J. Als-Nielsen, J. Bohr, and M. Nielsen, Synchrotron x-ray study of melting in submonolayer Ar and other rare-gas films on graphite, Phys. Rev. B **25**, 7765 (1982).

[24] P. A. Heiney, R. J. Birgeneau, G. S. Brown, P. M. Horn, D. E. Moncton, and P. W. Stephens, Freezing Transition of Monolayer Xenon on Graphite, Phys. Rev. Lett. **48**, 104 (1982).

[25] K. Zahn, R. Lenke, and G. Maret, Two-Stage Melting of Paramagnetic Colloidal Crystals in Two Dimensions, Phys. Rev. Lett. **82**, 2721 (1999).

[26] U. Gasser, C. Eisenmann, G. Maret, and P. Keim, Melting of crystals in two dimensions, Chem. Phys. Chem. **11**, 963 (2010).

[27] K. J. Strandburg, Two-dimensional melting, Rev. Mod. Phys. **60**, 161 (1988).

[28] D. S. Fisher, B. I. Halperin, and R. Morf, Defects in the two-dimensional electron solid and implications for melting, Phys. Rev. B **20**, 4692 (1979).

[29] S. T. Chui, Grain-Boundary Theory of Melting in Two Dimensions, Phys. Rev. Lett. **48**, 933 (1982).

[30] S. T. Chui, Grain-boundary theory of melting in two dimensions, Phys. Rev. B **28**, 178 (1983).

[31] Y. Saito, Monte Carlo studies of two-dimensional melting: dislocation vector systems, Phys. Rev. B **26**, 6239 (1982).

[32] Y. Saito, Melting of Dislocation Vector Systems in Two Dimensions, Phys. Rev. Lett. **48**, 1114 (1982).

[33] K. J. Strandburg, Crossover from a hexatic phase to a single first-order transition in a Laplacian-roughening model for two-dimensional melting, Phys. Rev. B **34**, 3536 (1986).

[34] A. L. Thorneywork, J. L. Abbot, D. G. A. L. Aarts, and R. P. A. Dullens, Two-Dimensional Melting of Colloidal Hard Spheres, Phys. Rev. Lett. **118**, 158001 (2017).

[35] B. I. Halperin and D. R. Nelson, Theory of Two-Dimensional Melting, Phys. Rev. Lett. **41**, 121 (1978).

[36] H. Kleinert, Disclinations and first order transitions in 2D melting, Phys. Lett. A **95**, 381 (1983).

[37] M. Engel, J. A. Anderson, S. C. Glotzer, M. Isobe, E. P. Bernard, and W. Krauth, Hard-disk equation of state: first-order liquid-hexatic transition in two dimensions with three simulation methods, Phys. Rev. E **87**, 042134 (2013).

[38] S. Prestipino, F. Saija, and P. V. Giaquinta, Hexatic Phase in the Two-Dimensional Gaussian-Core Model, Phys. Rev. Lett. **106**, 235701 (2011).

[39] S. I. Lee and S. J. Lee, Effect of the range of the potential on two-dimensional melting, Phys. Rev. E **78**, 041504 (2008).

[40] Y.-W. Li and M. P. Ciamarra, Attraction Tames Two-Dimensional Melting: From Continuous to Discontinuous Transitions, Phys. Rev. Lett. **124**, 218002 (2020).

[41] O. Toledano, O. Gálvez, J. E. Alvarellos, and M. Pancorbo. Random Phase, a MMC program for bidimensional melting, https://github.com/UNEDSoftMatter/RandomPhase.

[42] J. E. Mayer and W. W. Wood, Interfacial tension effects in finite, periodic, two dimensional systems, J. Chem. Phys. **42**, 4268 (1965).

[43] B. Frenkel and D. Smit, *Understanding Molecular Simulations: From algorithms to applications*, (Academic Press, San Diego, 1996).

[44] W. Mickel, S. C. Kapfer, G. E. Schröder-Turk, and K. Mecke, Shortcomings of the bond orientational order parameters for the analysis of disordered particulate matter, J. Chem. Phys. **138**, 044501 (2013).

[45] M. Michel, S. C. Kapfer, and W. Krauth, Generalized event-chain Monte Carlo: constructing rejection-free global-balance algorithms from infinitesimal steps, J. Chem. Phys. **140**, 054116 (2014).

[46] J. Delhommelle, Simulations of shear-induced melting in two dimensions, Phys. Rev. B **69**, 144117 (2004).

[47] U. Agarwal and F. A. Escobedo, Yielding and shear induced melting of 2D mixed crystals of spheres and dimers, Soft Matter **8**, 5916 (2012).